american physiological society

JNP JOURNAL OF NEUROPHYSIOLOGY

J Neurophysiol 128: 1011–1024, 2022.
First published September 21, 2022; doi:10.1152/jn.00325.2022

INNOVATIVE METHODOLOGY

Control of Movement

Large-scale intramuscular electrode system for chronic electromyography and functional electrical stimulation

Nicole L. Holly,[1]* Brady A. Hasse,[2]* Katalin M. Gothard,[1,3,4] and Andrew J. Fuglevand[1,3]

[1]*Department of Physiology, College of Medicine, University of Arizona, Tucson, Arizona;* [2]*Graduate Program in Neuroscience, University of Arizona, Tucson, Arizona;* [3]*Department of Neuroscience, University of Arizona, Tucson, Arizona; and* [4]*Department of Neurology, College of Medicine, University of Arizona, Tucson, Arizona*

Abstract

To understand how the central nervous system (CNS) enacts movements, it seems important to monitor the activities of the many muscles involved. Likewise, to restore complex movements to paralyzed limbs with electrical stimulation requires access to most limb muscles. Intramuscular electrodes are needed to obtain isolated recordings or stimulation of individual muscles. As such, we developed and tested the stability of large arrays of implanted intramuscular electrodes. We implanted 58 electrodes in 29 upper limb muscles in each of three macaques. Electrode connectors were protected within a skull-mounted chamber. During surgery, wires were tunneled subcutaneously to target muscles, where gold anchors were crimped onto the leads. The anchors were then deployed with an insertion device. In two monkeys, the chamber was fixed to the skull with a titanium baseplate rather than acrylic cement. In multiple sessions up to 15 wk after surgery, electromyographic (EMG) signals were recorded while monkeys made the same reaching movement. EMG signals were stable, with an average (SD) coefficient of variation across sessions of 0.24 ± 0.15. In addition, at 4, 8, and 16 wk after surgery, forces to incrementing stimulus pulses were measured for each electrode. The threshold current needed to evoke a response at 16 wk was not different from that at 4 wk. Likewise, peak force evoked by 16 mA of current at 16 wk was not different from 4 wk. The stability of this system implies it could be effectively used to monitor and stimulate large numbers of muscles needed to understand the control of natural and evoked movements.

NEW AND NOTEWORTHY A new method was developed to enable long-lasting recording and stimulation of large numbers of muscles with intramuscular electrodes. Electromyographic signals and evoked force responses in 29 upper limb muscles remained stable over several months when tested in nonhuman primates. This system could be used effectively to monitor and stimulate numerous muscles needed to more fully understand the control of natural and evoked movements.

electrodes; electromyography; functional electrical stimulation; stability

INTRODUCTION

Virtually all forms of movement involve complex coordination across large numbers of muscles. Even ostensibly simple movements of individual fingers engage a wide array of muscles, many of which do not insert into the moving digit (1–4). Part of the reason for this complexity is that a large proportion of muscles cross multiple joints. For example, the flexor digitorum profundus, when active, will tend to cause simultaneous flexion at the elbow, wrist, and all the joints of digits 2–5. Consequently, to enable relatively isolated movements at single joints requires a delicate balancing act of engaging other muscles that counteract otherwise unwanted movements.

Most of the enormous body of work dedicated to understanding the control of movement has largely ignored this complexity. Instead, in many instances, each degree of freedom at a joint is considered to be operated upon by single-joint agonist/antagonist muscle pairs. Indeed, many theories of motor control are partially built upon these simplifications

*N. L. Holly and B. A. Hasse contributed equally to this work.
Correspondence: A. J. Fuglevand (fuglevan@email.arizona.edu).
Submitted 29 July 2022 / Revised 13 September 2022 / Accepted 14 September 2022

(see, e.g., Refs. 5–11). And although important insights into the control of movement have been gained through these simplifications, a deeper understanding of how the brain and spinal cord dynamically regulate movements would seem to necessitate tracking the electromyographic (EMG) activities of many muscles. This, however, turns out to be extraordinarily difficult. This is partly because many muscles are deep and are not accessible with surface electrodes. Consequently, simultaneously recording the activities of the ~30 muscles that just move the arm, for example, becomes intractable in human subjects.

An important exception in this regard has been the work carried out in nonhuman primates, particularly in the context of recording brain activity during voluntary movements. These studies involved both percutaneously inserted and surgically implanted electrodes in 12–24 upper limb muscles (12–18). Typical durations over which these implants provided stable EMG recordings were 4–12 wk, although epimysial electrodes used by Miller et al. (16) were stable for up to 1 yr. Although usually not reported, the most likely causes of recording failure include migration of electrodes out of muscles, breakage of electrode leads, and infections at the connector interface. Given the valuable animal model and enormous investment in training animals to perform various tasks, this relatively modest electrode life span undercuts the extent of useful information that otherwise could be obtained and necessitates the use of additional animals.

To address these shortcomings, Cheney and colleagues modified methods used previously to chronically implant pairs of electrodes in 24 upper limb (19) and 20 lower limb (20) muscles in rhesus macaques. Two methods were used: one involved a modular system with externalized electrode connectors situated on the upper arm, and the other used a connector mounted to the skull with dental acrylic. Electrodes (bared ends of multistranded stainless steel wire) were inserted into muscles with hypodermic needles into which electrodes had been backloaded and folded over to form a hook. Excess lead was placed subcutaneously to provide strain relief to accommodate limb movements. EMG recordings with these methods were impressive and long-lasting: 6–10 mo for the upper limb (19) and 12–31 mo for the lower limb (20).

Despite the success of those methods, there nevertheless were some drawbacks. For the arm-based connector system, animals needed to be sedated about every 2 wk to have fur and hair shaved from the skin on the arm to replace the tape securing the connectors to the skin. In addition, to prevent animals from picking at the connectors and potentially damaging the implant, monkeys had to continuously wear metal-reinforced jackets. Furthermore, ribbon cables that ran from the connectors on the arm to the recording equipment might impede free arm movements during certain experiments and could lead to significant movement artifacts in EMG recordings. As such, that type of system would seem to work best for activities involving limited arm movement. The advantage of the skull-based connector system was that the entire implant was subcutaneous and therefore there was no need for the animal to wear a primate jacket and no need to regularly retape connectors. A disadvantage of such skull mounting is that the acrylic cement (polymethyl methacrylate, also known as dental cement) used to fix the connector can leave small gaps between bone and the implant. Such gaps can be a nidus for infections that gain entry at the acrylic-skin interface to cause bone necrosis and implant failure (21, 22). Finally, both methods used hooked wires to anchor electrodes in muscle. Such hooked wires provide minimal resistance to electrode displacement out of the target muscle. It is important to note that examination of EMG signals by itself is not diagnostic for electrode migration because displaced electrodes could still readily detect muscle activities from interfascial spaces.

Here we report on a method that adapts and addresses some of the limitations of the approach used by Cheney and colleagues (19, 20). Namely, our approach uses an acrylic-less, biocompatible, skull-based connector system with fully subcutaneous electrodes. In addition, electrode migration is minimized with small gold-plated anchors attached to the electrode leads. Finally, the system is relatively efficient to implant and thereby minimizes surgical time. We have recently used this system successfully in a long-term study involving EMG recording and functional electrical stimulation of 29 upper limb muscles in rhesus macaques (23).

METHODS

Subjects

Three adult male monkeys (*Macaca mulatta*, 10–13.5 kg, ages 7–11 yr), that were participants in a different study (23), were the subjects for this project. One monkey (*monkey E*) was implanted with acrylic cement mounting of the electrode-connector chamber on the skull, whereas the other two (*monkeys A* and *M*) were implanted with a titanium platform for mounting the chamber on the skull. All procedures complied with guidelines for the use of nonhuman primates in research and were approved by the institutional animal care committee.

Electrode Leads

Sixty multistranded 316 stainless steel wires coated with Teflon (AS 633, outside diameter = 0.3 mm; Cooner Wire, Chatsworth, CA) were soldered to a 64-channel electrode interface board (EIB-36-16TT; Neuralynx, Bozeman, MT) consisting of two 32-channel connectors. Two wires were designated for each of 29 arm muscles to enable bipolar EMG recording and, in some cases, bipolar stimulation. The two additional wires were included as backups in case of malfunction or damage during surgery. The lead of a large disk electrode (silver-silver chloride, ~1-cm diameter), which served as a ground and stimulus return, was also soldered to the board. The connector board was then mounted into a cylindrical chamber with a removable lid that was secured with screws. The electrodes (~70 cm in length) emerged from the base of the chamber. The chamber (~30-mm diameter) was machined from Delrin (Dupont, Wilmington, DE) for *monkey E* and was three-dimensional (3-D) printed with VisiJet Crystal (3 D Systems, Rock Hill, SC) for *monkeys A* and *M*. After the connector pin to which each wire was soldered was identified, the distal ends of the wires were painted with a four-band color code designating the target muscle for easy visualization during surgery. The color code also distinguished between the two electrodes destined for

each muscle needed for bipolar recording. Once the color codes were applied to all wires, they were grouped according to target muscle groups and bundled with sutures at a few positions along their length. These bundles were then grouped into two sets: one destined for muscles in the back and dorsal regions of the upper arm (blue, Fig. 1*A*) and forearm (Fig. 1*B*) and one destined for muscles on the ventral aspect of the chest and arm (yellow, Fig. 1*C*). The ground electrode (green, Fig. 1*A*) was kept separate from the two sets. All the wires were then wrapped around and secured

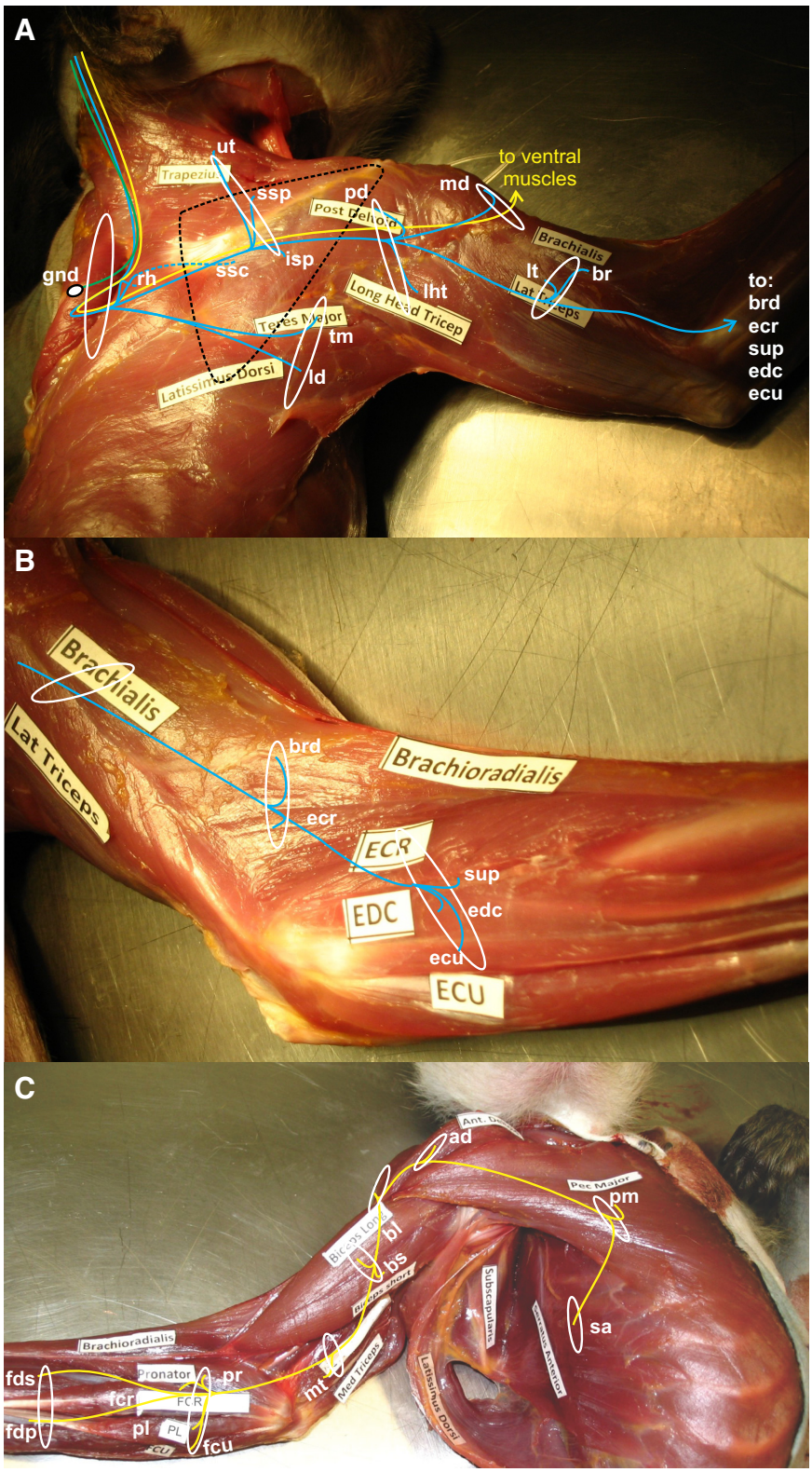

Figure 1. Dissection showing implanted muscles and routing of electrodes. Dissection was performed on a cynomolgus (*Macaca fascicularis*) monkey, after harvesting of organs for a different study. White ovals indicate approximate locations of incisions. Terminations of lines indicate sites where electrode pairs were inserted into muscles. *A*: dorso-lateral view of back and upper arm. Approximate position of the scapula is indicated by black dashed line. The ground (gnd, green) and 2 main bundles (dorsal, blue; ventral, yellow) were pulled through to an incision between the scapulae from the chamber on the skull. Subscapularis (ssc) was approached by dorsally elevating the medial edge of scapula and inserting electrodes into ventral surface of scapula with a long 21-gauge needle. Ventral bundle was pulled through to incision over the medial deltoid (md). br, Brachialis; brd, brachioradialis; ecr, extensor carpi radialis; ecu, extensor carpi ulnaris; edc, extensor digitorum communis; isp, infraspinatus; ld, latissimus dorsi; lht, long head triceps; lt, lateral triceps; pd, posterior deltoid; rh, rhomboids; ssp, supraspinatus; sup, supinator; tm, teres major; ut, upper trapezius. *B*: dorsal forearm showing continuation of dorsal bundle. *C*: ventro-lateral view of arm showing incisions and destinations of electrode pairs. ad, Anterior deltoid; bl, biceps brachii long head; bs, biceps brachii short head; fcr, flexor carpi radialis; fcu, flexor carpi ulnaris; fdp, flexor digitorum profundus; fds, flexor digitorum superficialis; mt, medial triceps; pl, palmaris longus; pm, pectoralis major, pr, pronator teres; sa, serratus anterior.

within a flexible plastic thread bobbin (XTL-6103; Beadsmith, Carteret, NJ) to protect the wires during the initial stages of the surgery and to prevent tangling. The implant was then gas sterilized in advance of surgery.

Surgery Using Acrylic Cement to Mount Chamber

Monkeys were sedated in their home cage with ketamine HCl (10–15 mg/kg intramuscular), and then a surgical level of anesthesia was achieved and maintained with isoflurane (1.5–2% in 100% oxygen) delivered through an endotracheal tube. Hair and fur were removed from the skull, right arm, and right upper quadrant of the torso. The monkey's head was then fixed in a stereotaxic frame for the initial phase of the surgery. Under sterile conditions, a transverse incision was made on the top of the skull, and the temporalis muscles and fascia were resected and the periosteum removed to prepare the site for mounting of the cylindrical chamber containing the electrode connectors. Ten titanium screws were inserted into the skull to anchor dental acrylic cement used to secure the chamber. The chamber was placed on the skull, and a Teflon dam was put in place to encircle the outside of the bone screws. Dental cement was poured in layers into the area within the Teflon dam, which sealed and attached the chamber to the skull of the monkey. After the cement hardened, the Teflon dam was removed. The wires exited the chamber posteriorly on the skull near the occipital ridge. They were then unwound from the bobbin and pulled through to an incision (~4 cm) made between the two scapulae (19, 20). The ground electrode was inserted into a blunt-dissected pocket at the midscapular incision. The other wires were then rewound around the bobbin and inserted into the pocket in the midscapular incision to protect them during repositioning and redraping of the animal. This incision was temporarily closed with a few surgical staples. The incision on the skull was closed with suture, and the head was removed from the stereotaxic frame.

The skin overlying the arm, shoulder, back, and neck was then prepared for surgery with antimicrobial scrub. The animal was first positioned in semiprone position with the shoulder abducted and the elbow flexed. A set of incisions were made at locations above target dorsal muscles for electrode insertion (see ovals in Fig. 1, *A* and *B*). With blunt dissection, wire bundles were tunneled under the skin from one incision to the next until they reached their target incision, where the wire ends were exteriorized.

Electrodes and Electrode Insertion

Beginning at the most distal incision, brief trains of stimulation (40 Hz, biphasic, 250 μs/phase, 1–3 mA) through a low-impedance tungsten electrode were first used to identify a site that evoked robust contraction in the desired muscle. The corresponding electrode wire was cut to a length so there was ~5–7 cm of wire emerging from the incision. About 2 mm of insulation was then removed from the end of the wire with a sterilized thermal wire stripper (Hotweezers M-10; Meisei Tools LLC, Thousand Oaks, CA). A gold electrode anchor (~1 × 7 mm) (Fig. 2*A*) was crimped onto the lead with a crimping tool (AFM8; Daniels Manufacturing, Orlando, FL), thereby making electrical contact between the lead and anchor. The anchor consisted of a crimp terminal pin (3922; Mill-Max, Oyster Bay, NY) with the pin removed. Anchors were used to increase surface area and shear friction and to help prevent electrode migration. Furthermore, the anchor itself served as the electrode, having a larger surface area (and reduced overall electrical impedance) than that of just bared lead wire.

The anchor was fed into the opening of a custom-built insertion tool made of a 14-gauge needle with a narrow slot cut along the length (Fig. 2*B*) through which the lead exited (Fig. 2*C*). This tool was then inserted alongside the tungsten electrode that served as a guide before the tungsten electrode was removed. Stimuli were then delivered through the insertion tool (fully insulated with Konform AR; Chemtronics,

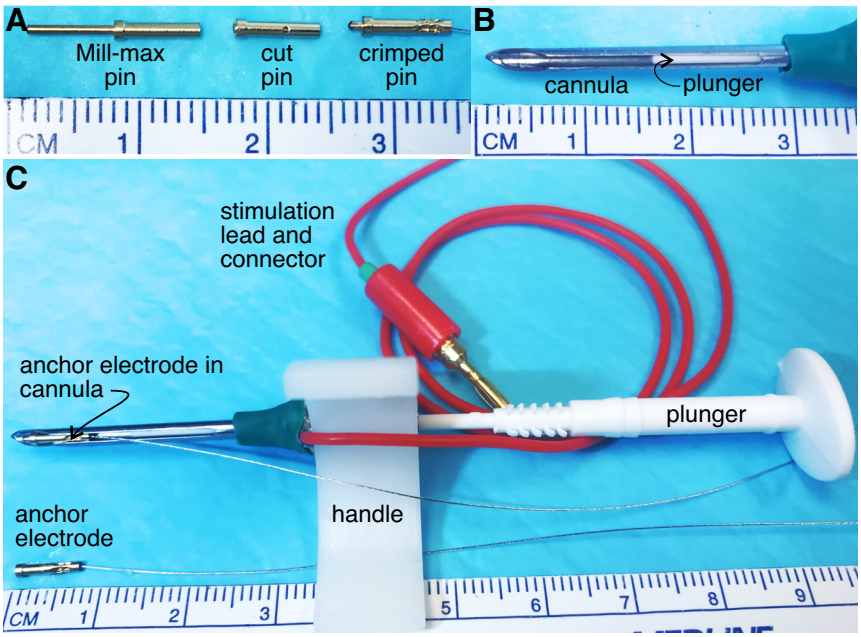

Figure 2. Tool for inserting anchor electrodes. *A*: anchor was a gold terminal pin (3922 Mill-Max) that had the pin portion removed (cut pin). During surgery, the sterilized anchor was crimped to 0.3-mm (outside diameter) electrode wire that had a small amount of insulation removed at the tip. *B*: cannula of the insertion tool with a slot cut along the length. The tip of the plunger can be seen retracted part way up into the cannula to accommodate the placement of the anchor in the tool. *C*: during surgery, the anchor was fed into the cannula of the insertion tool with the lead exiting through a slot cut along the length of the cannula. The cannula was electrically insulated except for the tip, through which stimuli could be delivered via the stimulation lead attached to the cannula. When stimulation provoked robust contraction in the target muscle, the anchor was deployed by pushing a plunger through the cannula.

Kennesaw, GA, except for the tip of the needle) to evoke contraction in the target muscle and to verify optimal placement. With a plunger that pushed back through the needle, the anchor was deployed to the same location as the needle tip (Fig. 2). The insertion tool was removed, and stimuli were then delivered through the connector on the skull to the anchor to verify robust contraction in the target muscle. If stimulation activated the wrong muscle, activated multiple muscles (perhaps because of placement near a peripheral nerve), or had a high threshold, the anchor was removed, a new insertion site identified, and the process repeated. Trains of stimulus pulses (1-s trains, 40 Hz) were then delivered every 2 s with stimulus amplitude incrementing in 0.2-mA steps. The threshold current was noted based on the intensity that first evoked a detectable contraction, identified by palpation or visible skin deformation over the target muscle. This process was then repeated for the other electrode for a given muscle and for all other muscles. The distance between insertion sites for a bipolar electrode pair was ~5–10 mm.

The one exception to this method was for the subscapularis muscle. It sits on the ventral surface of the scapula, making it difficult to approach with the insertion tool. For this muscle, we used the hooked-wire method and back-fed ~5 mm of deinsulated wire into the mouth of a long 21-gauge needle. The lead was then folded along the outside of the needle. The medial edge of the scapula was manually reflected dorsally and the needle advanced from the midline incision under the scapula until it contacted its ventral surface, whereupon the needle was removed, leaving the electrode in place.

Once all the electrodes were inserted at a particular incision site, slack from all the wires was tucked subcutaneously into the incision and either quill-type (Quill Monoderm; Surgical Specialties, Westwood, MA) or 2.0 and 3.0 coated Vicryl sutures (Ethicon, Somerville, NJ) were used to close the incision. This process was continued at the next most distal site until all the electrodes on the dorsal side were inserted and the incisions closed. The monkey was then turned over into a semisupine position to expose the ventral side. The animal was then reprepped and redraped. Incisions were made at sites on the ventral side overlying target muscles (Fig. 1*C*), the wires were tunneled subcutaneously to the appropriate incisions, and electrodes were inserted as described above.

As the animal was weaned off the anesthesia, surgical dressings (Tegaderm; 3M, Maplewood, MN) with antimicrobial cream were applied to the incision sites. While the monkey was still anesthetized, the implanted arm was folded across the abdomen (i.e., elbow was flexed ~90° and the shoulder fully internally rotated). Heavy-duty, wide vet wrap was then used to secure the implanted arm to the torso by repeatedly encircling the body and arm with the wrap. To prevent the animal from removing the wrap, the monkey was placed in a primate jacket. The jacket enabled free movements of the nonimplanted arm but impeded access to the wrap. Immobilization of the limb was maintained for a period of 1 wk to help anchor the electrodes in place (24).

Despite stable recordings from this animal (*monkey E*) over a period of 6 mo, an untreatable infection (methicillin-resistant *Staphylococcus aureus*) developed under the acrylic cement mount securing the chamber to the skull. This caused severe bone degeneration requiring the animal to be euthanized. This negative outcome prompted us to develop a skull mounting system that did not involve acrylic cement. The other two monkeys were implanted with this new design, described below.

Titanium Baseplate

For the new implant design, we adapted a method described by Blonde et al. (25). This method first involved fabrication of tissue-friendly titanium baseplates that conformed exactly to the contours of each animal's skull based on computed tomography (CT) image data. Those data were used to construct baseplates for each animal with 3-D printing of titanium (Gray Matter Research, Bozeman, MT). Imprinted in the baseplate was a recessed region for securing the chamber protecting the two electrode connectors (Neuralynx) to the baseplate (Fig. 3*A*). A groove was also fabricated into the baseplates that served as a channel through which electrodes ran from inside the chamber to a posterior

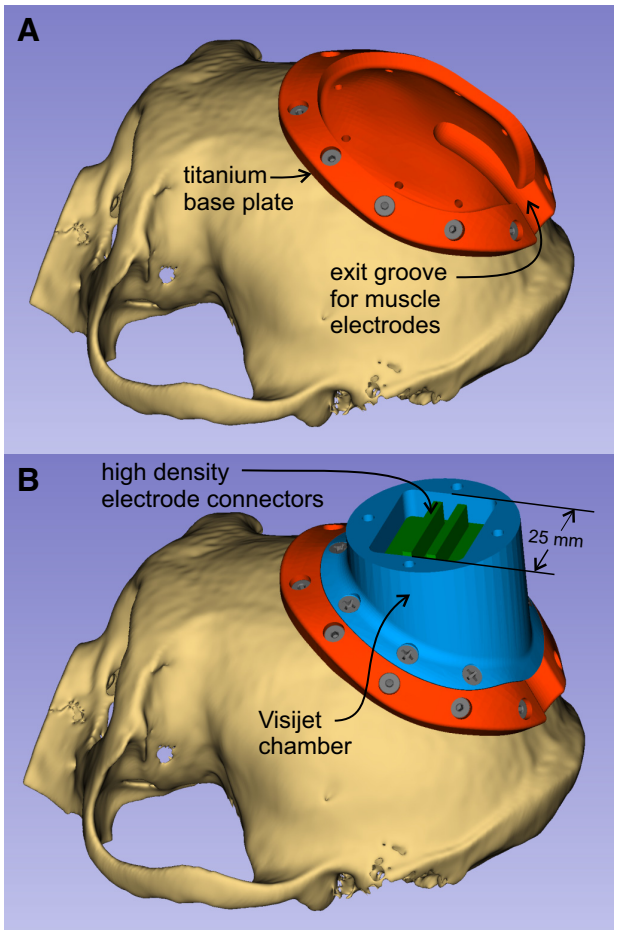

Figure 3. *A*: titanium baseplates were custom fabricated for each monkey based on computed tomography (CT) images of the skulls. The plate possessed a recessed region to accept the chamber. A groove at the back of the plate provided a channel for the electrodes that exited the base of the chamber. The plate was surgically implanted first. *B*: several weeks later (after titanium has become well integrated into skull), a biocompatible (VisiJet) chamber, containing high-density electrode connectors and electrodes, was installed on the plate.

exit site near the occipital crest (Fig. 3*A*). Chambers were 3-D printed from VisiJet (3 D Systems) with a flange that sat flush to the titanium surface and possessed through-holes for securing the chamber to the baseplate with titanium screws (Fig. 3*B*).

Titanium Baseplate Surgery

Implantation of the baseplate system involved two separate surgeries, one to install the titanium baseplate on the skull and a second one in which the chamber was fixed to the baseplate and the electrodes inserted into the muscles. About 6–8 wk was allowed between the two surgeries for baseplates to osseointegrate before electrode implantation surgery. For the baseplate surgery, monkeys were sedated and anesthetized as described above. Fur and hair were removed from the skull, and the monkey's head was fixed in a stereotaxic frame. Under sterile conditions, a C-shaped incision was made, and the skin flap was reflected posteriorly. The temporalis muscles and fascia were resected to prepare the site for mounting of the titanium baseplate. The distance from the occipital crest to the posterior aspect of the baseplate, measured from the CT images used in the baseplate design (Fig. 3*A*), was measured in surgery to identify the approximate placement site for the plate on the skull. The baseplate was then manually maneuvered until it registered well on the skull. Eleven titanium screws were used to secure the plate to the skull. A smooth cap (VisiJet), the top of which was flush with the titanium surface and with a footprint identical to that used for the chamber, was then screwed into the depression in the titanium plate to eliminate high-pressure regions along the inner edge of the titanium plate. The skin flap was closed with 2.0 and 3.0 coated Vicryl suture. The animal was then weaned off anesthesia and recovered.

Electrode Implantation Using Titanium Baseplate

Because of unrelated postponements, chamber and electrode implantation did not occur until 12 (*monkey M*) and 13 (*monkey A*) wk after baseplate installation. Monkeys were sedated, shaved, prepped, and anesthetized as described above. The head was placed in a stereotaxic frame, and a circular incision was made in the skin just large enough to expose the screws of the protective cap sitting in the recessed region of the titanium plate. Those screws were unfastened and the cap removed. The electrodes attached to the chamber were unspooled from the bobbin and tunneled posteriorly to an incision between the scapulae. The chamber was then easily attached to the titanium plate with screws into tapped holes in the plate. The skin surrounding the encasement was closed with drawstring suturing. The remainder of the surgery was performed in the same manner as the first implantation method.

Electromyography Testing

Once implanted, all three animals participated in a set of experiments for a different study. That study involved recording of limb kinematics and EMG signals from the implanted muscles while the monkeys made complex arm movements (23). Two of the monkeys also underwent several sessions involving functional electrical stimulation through the electrodes of the implanted muscles to evoke complex limb trajectories while they were temporarily paralyzed with anesthesia. In addition, as one way to evaluate the stability of the implanted electrodes, EMG signals were recorded in several sessions while all three monkeys performed multiple trials of the same simple task. The task involved the monkey reaching his hand from a start box (positioned near the thigh of the monkey) to a morsal of food held directly in front of and at eye level of the monkey; the monkey grasped the morsel, transported it to his mouth, and then returned his hand to the start box. To record EMG activity, two lightweight cables were attached to the connectors within the skull-mounted chamber. These cables were routed to a set of four eight-channel differential amplifiers (Neuralynx). EMG signals were amplified at a gain of 1,000, band-pass filtered from 100 to 475 Hz, and digitally sampled at ~3,000 Hz per channel with a computerized data acquisition system (Spike2; Cambridge Electronics Design, Cambridge, UK). In off-line processing (MATLAB; MathWorks, Natick, MA), EMG signals were full-wave rectified, low-pass filtered (3 Hz), and downsampled to 120 Hz/signal to match kinematic data.

Stimulation

As another means to evaluate electrode stability, we recorded the relation between stimulus intensity and evoked isometric force for all 58 electrodes in two monkeys (*A* and *M*) at 4, 8, and 16 wk after electrode implantation. To do this, we used a method detailed previously (23, 26). In brief, monkeys were anesthetized with isoflurane and placed into a modified infant car seat in a seated position. A human pediatric cervical collar was used to maintain the head in an upright position. The cervical collar was secured to the car seat, and straps situated midway between the neck and shoulder and across the torso secured the animal to the chair. A single multiaxis isometric transducer (45E; JR3, Woodland, CA) was separately fixed to the wrist/hand, the forearm, or the upper arm to record the three-dimensional components of evoked isometric forces associated with muscles acting on each of those segments. In each case, limb and body segments proximal to the tested segments were immobilized with Velcro straps.

Stimuli were delivered through the skull-mounted connector to each electrode separately with a programmable multichannel stimulator (STG4008; MultiChannel Systems, Reutlingen, Germany). Stimuli were single, biphasic (cathode leading, 250 μs/phase) rectangular pulses delivered at 1-s intervals that incremented from 0.2 mA to 2.0 mA in 0.2-mA steps and then from 3 mA to 16 mA in 1-mA steps. We used small increments of current at the low end of stimulus intensities to capture, with good resolution, the minimum current needed to just evoke a contractile response. In addition, we used single stimuli and evoked twitches rather than trains of stimuli and tetanic contractions to reduce the time monkeys were under anesthesia and to minimize the possibility of fatigue. Because we were interested in evaluating stability of evoked responses across sessions, the order in which stimuli of different amplitudes were delivered was not randomized but kept the same to facilitate fairer comparisons across sessions. The return electrode was the large ground electrode

situated subcutaneously between the scapulae. In postprocessing, the resultant peak twitch force evoked by each stimulus was determined.

Data Analysis

To evaluate stability in EMG signals over time, rectified and smoothed EMG signals were first time normalized to the duration of each phase (reach, grasp, to mouth, back to start box) of the simple reaching task. This helps to account for some of the variability in time spent on each phase of the task across trials and subjects (rather than variability in EMG signal per se). For most cases, a machine learning algorithm was used to identify the event times, segregating the phases of a reach from kinematics recorded with a 6-degree of freedom sensor (Liberty; Polhemus, Colchester, VT) attached to the back of the hand with elastic wrap. These time-normalized signals were then averaged across all trials within a session. Amplitudes of the EMG signals were not normalized but kept in absolute units (mV) to highlight any changes in strength of detected signals that might have arisen because of electrode migration across sessions. To quantify the degree of variability across sessions in these time series, we used the coefficient of variation (CV = standard deviation/mean), a unitless measure indicating the extent of variability in relation to the mean level. CV values were calculated at each time point across multiple session-averaged EMG signals for a given muscle. The mean of the resulting array of CV values (1 for each time point across the duration of the task) was then calculated for each muscle and each monkey. This provided a simple measure that represented the variation across multiple trials (i.e., sessions) of the same time-varying signal.

For the stimulus-evoked twitches, we first identified the minimum current needed to evoke a detectable force response. We tried several methods to determine the threshold level automatically and objectively, including the conventional approach of identifying threshold based on multiple standard deviations above the prestimulus average value. However, because of the relatively small number of baseline values available for those calculations before stimulus delivery, and substantial respiratory artifact contaminating the baseline in some cases, that approach was not reliable. The method that seemed most reliable involved using the distinctive shape of a twitch to discern threshold. Starting with the force responses to the largest currents and working backward toward the weakest current, we progressively calculated the average correlation coefficient between a given response and the responses to the three higher increments in current. When the average correlation coefficient dropped below 0.5, that response was considered not "twitchlike" and the next higher current was deemed threshold. In addition, we measured the peak twitch force at 16 mA of current as another assessment of stability of evoked responses. These measures were made for each of the 58 electrodes in two monkeys at three time points following the surgery (4, 8, 16 wk). To determine the degree of change in these measures over time, we normalized their values at 8 and 16 wk as a percentage of that recorded at 4 wk. A simple one-sample t test was performed to determine whether the values at 8 and 16 wk were different from 100%. Values are reported as means ± one standard deviation.

RESULTS

Figure 4*A* shows a radiograph of the implanted system using the titanium baseplate. The screws seen at the top of the baseplate are those that held the lid onto the chamber. The disk near the midline is the ground/return electrode. Individual anchor electrodes can be seen distributed throughout

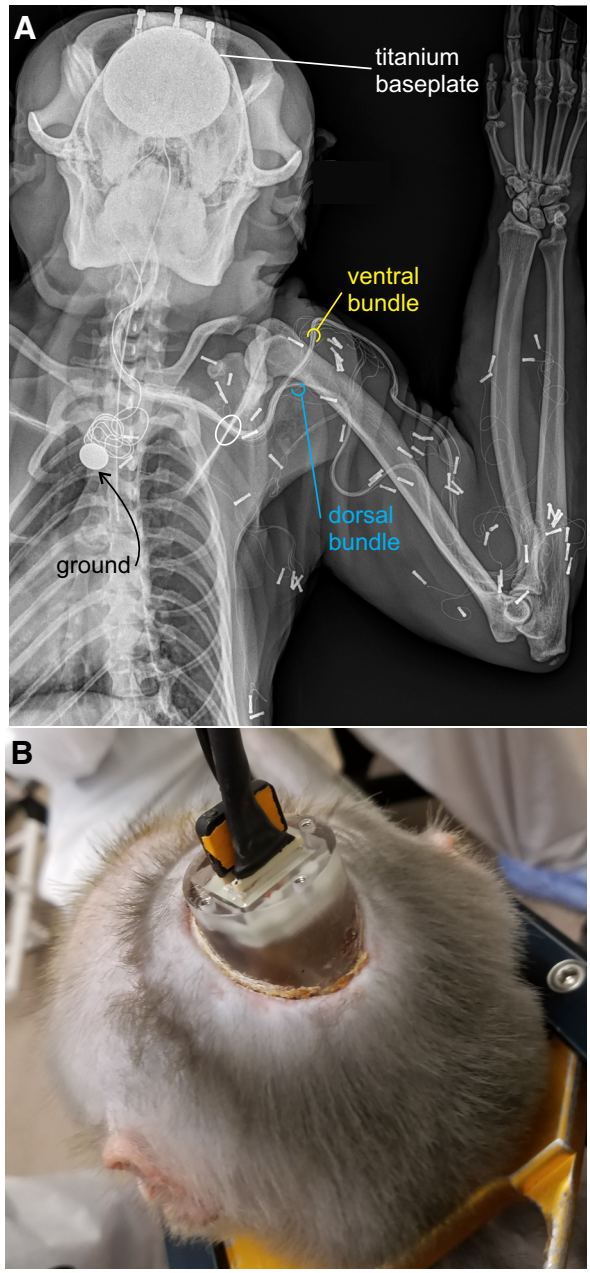

Figure 4. *A*: radiograph showing implanted system. Titanium baseplate is seen on the skull. Wire bundle passed from chamber on the skull to a midline position where it was routed laterally. Eventually, the main bundle separated into 2 bundles destined for dorsal and ventral muscles of the arm. Individual wires can be seen terminating in anchors implanted in muscles. A disk electrode served as ground and as the return electrode for stimulation. The oval over the spinous process on the scapula indicates a region where skin breakdown eventually occurred. *B*: photograph of chamber 4 wk after its implantation with cables attached to connector imbedded in chamber. Skin at base of chamber is healthy, with a tight seal between the chamber and skin.

the back, chest, and arm. The dorsal and ventral electrode bundles (see Fig. 1) are indicated. The oval indicates a site where the main electrode bundle crossed over the spinous process of the scapula (discussed below).

Figure 4*B* is an image of the chamber, mounted on the titanium baseplate, with cables running to EMG amplifiers, taken 4 wk after the implant surgery. The skin at the margin of chamber made a tight seal, was healthy, and had no signs of infection. Over time in both monkeys, however, the skin retracted away from the underlying flange of the VisiJet chamber and, by 12 wk after surgery, from the titanium baseplate. Nevertheless, the skin margin remained healthy, clean, and uninfected for the lifetime of the implant in both monkeys.

Figure 5 depicts an example EMG recording taken about 5 wk after surgery. This recording was taken while the monkey was making free arm movements. All 29 channels provided low-noise, distinct, and detailed signals (e.g., single-motor unit potentials are discernible in some muscles) with minimal indication of movement artifacts or cross talk. To quantify the extent of cross talk, we performed cross-correlation analysis between all pairs of EMG signals (27) recorded in one monkey over a 20-min session while the monkey made complex arm movements (23). The peak correlation value near time zero (±2 ms) was used to indicate the magnitude of volume-conducted cross talk (27). Figure 6 shows the outcome of that analysis. Muscles are ordered in the matrix of Fig. 6 roughly according to their arrangement in the limb, with proximal muscles in the top rows and left columns and distal muscles in the bottom rows and right columns. Therefore, elements near the main diagonal in the matrix represent pairs of muscles physically near to one another. Overall, cross-correlation values were small (average peak correlation coefficient = 0.021 ± 0.014) even for most neighboring muscles. This indicates that only a small percentage on average (~2%) of the signal picked up in one muscle was

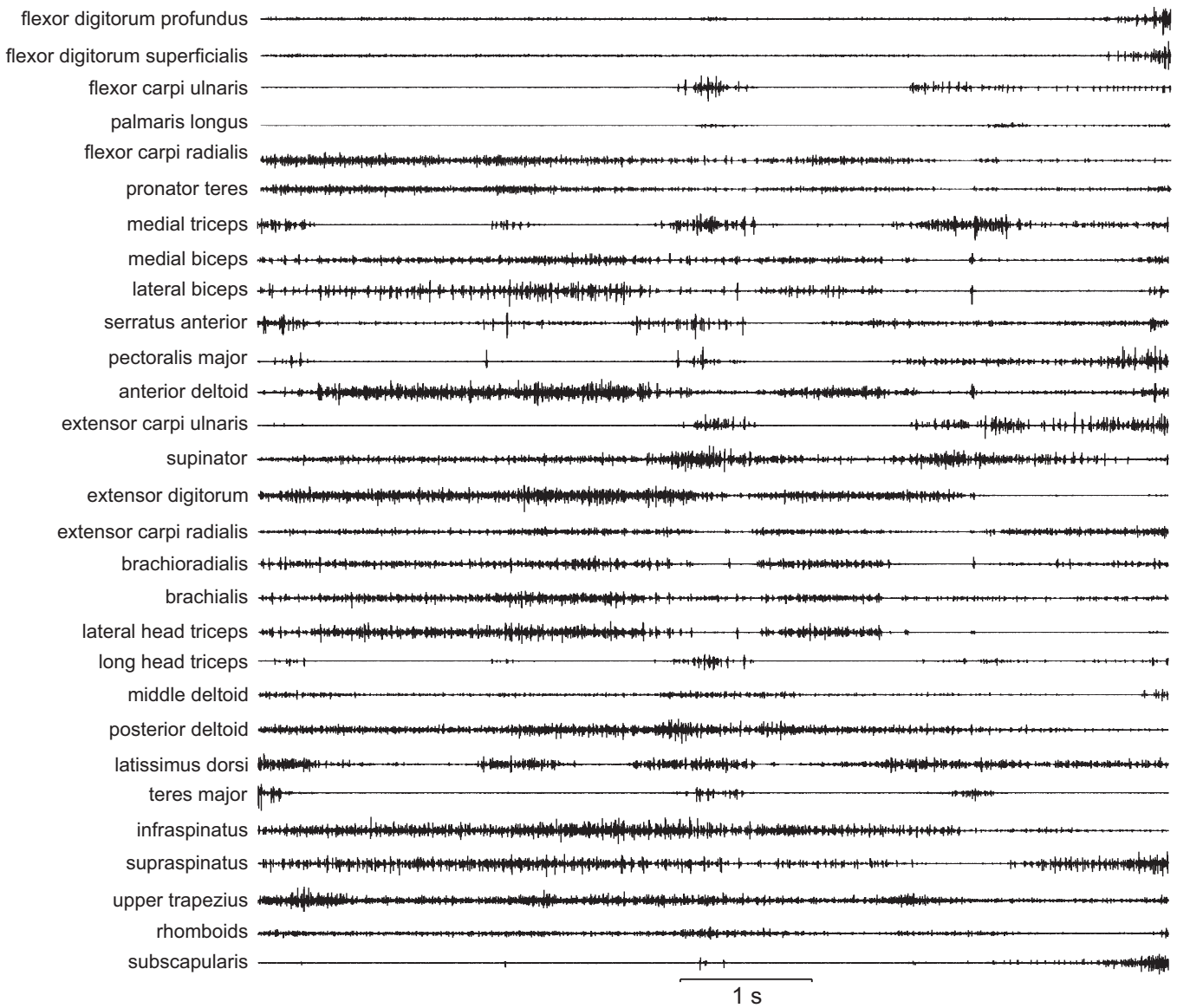

Figure 5. Example unprocessed electromyographic (EMG) recordings from 29 arm muscles during free arm movements.

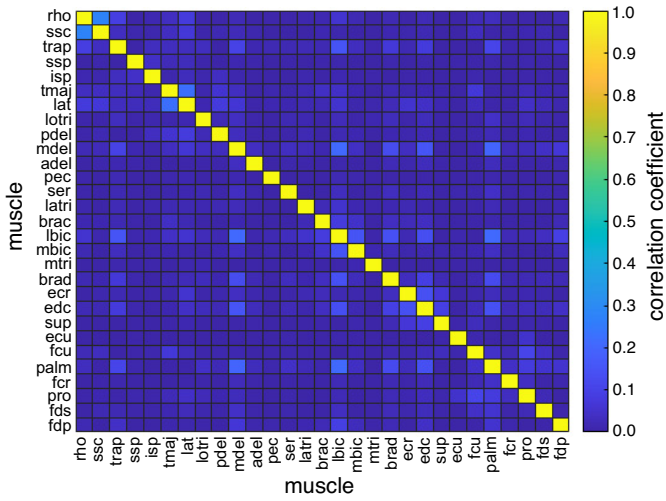

Figure 6. Matrix of peak cross-correlation values between all pairs of electromyographic (EMG) signals recorded in 1 monkey during a 20-min recording session involving complex arm movements. Matrix is arranged with proximal muscles in the *top* rows and *left* columns, whereas distal muscles are in the *bottom* rows and *right* columns. adel, Anterior deltoid; brac, brachialis; brad, brachioradialis; ecr, extensor carpi radialis; ecu, extensor carpi ulnaris; edc, extensor digitorum communis; fcr, flexor carpi radialis; fcu, flexor carpi ulnaris; fdp, flexor digitorum profundus; fds, flexor digitorum superficialis; isp, infraspinatus; lat, latissimus dorsi; latri, lateral head of triceps; lbic, lateral (long head) biceps; lotri, long head of triceps; mbic, medial biceps; mdel, middle deltoid; mtri, medial head of triceps; palm, palmaris longus; pdel, posterior deltoid; pec, pectoralis major; pro, pronator teres; rho, rhomboids; ser, serratus anterior; ssc, subscapularis; ssp, supraspinatus; sup, supinator; tmaj, teres major; trap, upper trapezius.

likely due to signal emanating from another muscle or from common 60-Hz noise.

Of the 176 anchor electrodes implanted in three monkeys, 8 electrodes failed (4.5%). Evidence of failure was primarily based on a marked increase in stimulus threshold. At implantation, all electrodes had stimulus threshold values below 3.5 mA. In the case of the failed electrodes, threshold values exceeded 8 mA at 4 or 8 wk after surgery. This was sometimes accompanied, but not always, by noisy EMG signals from the associated muscles. We believe, but cannot be certain, that the main reason for electrode failure was breakage somewhere along the length of the electrode lead. However, two of the failed electrodes were implanted without anchors in the subscapularis muscle. In these cases, failure could have been due to electrode migration out of the muscle. The EMG and evoked responses from the muscles associated with these failed electrodes were excluded from subsequent analyses. EMG analyses, therefore, involved 79 muscles from three monkeys, and evoked force responses included 109 electrodes from two monkeys.

EMG Stability

We assessed the stability of electrode implants by examining the patterns and amplitudes of EMG signals recorded over several sessions during the performance of the same simple task. Figure 7 shows example averages of rectified, low-pass filtered EMG signals from 12 muscles during 10 different sessions (spanning 11 wk) of the reaching task in *monkey E*. Figure 7, *bottom*, shows video frames demarking different stages of the task (reach, grasp, to mouth, back to start box). All traces for all muscles are shown on the same nonnormalized vertical scale (in mV).

For the most part, these signals were highly consistent across sessions. The average (±SD) coefficient of variation (CV) value across all muscles for this monkey (*E*) was 0.17 ± 0.08. When data from *monkey A* (31 sessions, spanning 15 wk) and *monkey M* (11 sessions, spanning 5 wk) were included, the average CV was 0.24 ± 0.15, with median = 0.24, and range 0.03–0.75. These levels of CV are on the same order as that reported for lower limb muscles during consecutive walking strides recorded within single experimental sessions with surface electrodes in humans (28). Collectively, such low CV values in nonnormalized EMG signals over multiple recording sessions suggest that the implanted anchor electrodes remained stable and durable over time.

Stability of Evoked Forces

An independent means to evaluate the stability of implanted electrodes is to characterize the relation between stimulus intensity and evoked isometric force (29). Indeed, even small shifts in electrode position within a muscle can cause marked changes in evoked force (30). Accordingly, we recorded evoked twitch forces for both electrodes in all muscles across a range of stimulus intensities from 0.2 to 16 mA on three separate occasions: at 4, 8, and 16 wk after implant surgery in two monkeys. From such responses, we made two measurements: the stimulus current associated with threshold and the resultant peak twitch force associated with the strongest stimulus strength (16 mA). We then normalized values recorded in *week 8* and *week 16* as a percentage of those recorded in *week 4*.

Figure 8 shows example evoked twitches in a single muscle (long head of triceps) at the three time points. Threshold responses are shown as the pink trace. For this example, threshold currents were 5, 4, and 5 mA for *weeks 4*, *8*, and *16*, respectively. As such, thresholds at *week 8* and *week 16* were 80% and 100% of that at *week 4*. The peak twitch forces evoked with a 16-mA stimulus at 4, 8, and 16 wk were 12.7, 14.7, and 16.1 N, yielding normalized responses of 116% and 127% for *weeks 8* and *16*, respectively.

Figure 9*A* depicts the mean (SD) normalized threshold across all electrodes and muscles and both monkeys. There was no significant change in threshold at *week 8* (106 ± 48%, $P = 0.197$, median = 100%) or at *week 16* (113 ± 47%, $P = 0.06$, median = 100%) compared with 100% associated with *week 4*. For *week 4*, the threshold current across all electrodes and muscles and both monkeys had a mean value of 2.5 ± 1.7 mA, median = 1.8 mA, and a range from 0.4 to 7.0 mA. Despite absence of systematic changes in threshold over the measurement period, there was still a fair amount of variability in these measures. The largest change was for palmaris longus at 16 wk, with a normalized value of 233%. In this case, the absolute change in threshold, however, was <1 mA, changing from 0.6 mA at *week 4* to 1.4 mA at *week 16*.

Figure 9*B* shows the mean (SD) normalized evoked force for 16-mA stimulation at *weeks 8* and *16*. The evoked force at *week 8* was significantly reduced (88 ± 42%, $P = 0.003$, median = 85%) compared with that at *week 4*. This reduction was seen in *monkey A* (76 ± 40%) but not in *monkey M* (102 ± 40%).

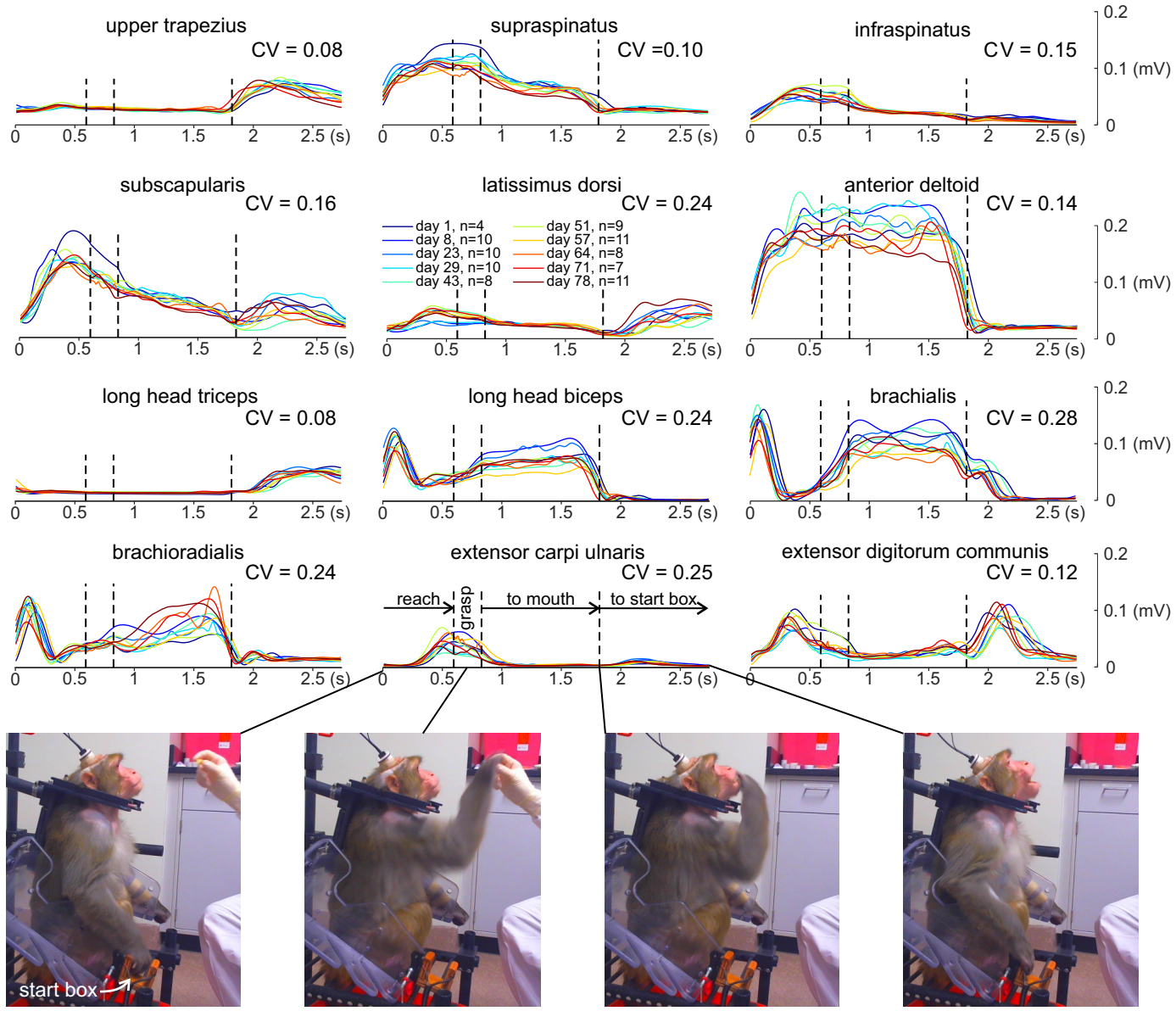

Figure 7. Stability of electromyographic (EMG) recording over 78 days during reaches to a food morsel. *Bottom*: images of monkey in start position, reaching to food morsel, grasping it, transporting it to mouth, and returning hand to the start box. *Top*: associated rectified and smoothed EMG from 12 example muscles recorded over 11 sessions. Each trace is the average of several trials (no. of trials shown in latissimus dorsi panel). Coefficient of variation (CV) across all recorded sessions is shown for each muscle.

For most muscles in *monkey A* at *week 8*, there was a consistent reduction in force across stimulus intensities (including 16 mA). The reason for this reduction is not clear. It could be that the positioning of this monkey in the testing apparatus at 8 wk was inconsistent with that of the other two sessions. Indeed, remounting an animal in a test apparatus within a session can cause significant changes in isometric force in response to nerve cuff stimulation (29). In *week 16*, the evoked forces were not significantly different from those at *week 4* (102 ± 26%, P = 0.467, median = 104%). Overall, these results suggest that over the 12-wk testing period the evoked responses to stimulation were reasonably consistent and suggest minimal electrode migration.

Long-Term Health of the Implants

As mentioned in METHODS, the animal (*monkey E*) implanted using dental acrylic to secure the chamber to the skull developed an untreatable bone infection and was euthanized 6 mo after implant surgery. In the other two monkeys (*A* and M) implanted with the titanium baseplates, the skin and bone surrounding the chamber remained healthy and without infection for the duration of the study. However, at ~6.5 mo after electrode implantation, *monkey A* developed a small skin ulceration near where the wire bundle traversed the occipital ridge on the posterior aspect of the skull that became infected. To treat this, the tissue surrounding the lesion was debrided and the wound closed

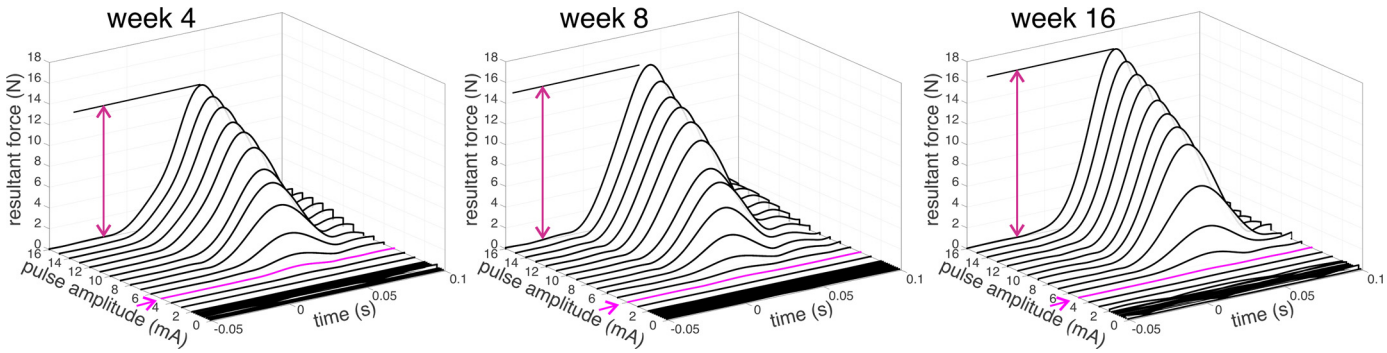

Figure 8. Example evoked twitches in response to stimulus pulses delivered to the long head of triceps that varied in intensity from 0.2 to 16 mA recorded at 4, 8, and 16 wk after implant surgery. Pink trace indicates identified stimulus threshold. Double-headed arrow indicates peak force in response to 16-mA current pulse.

with suture and antibiotics were initiated. The monkey then developed another lesion and infection ~1 mo later in the skin overlying the disk ground electrode, through which that electrode began to protrude. An incision was made adjacent to the lesion, the disk and wire were dissected from scar tissue and pulled back under the skin, and the incision was closed with suture. The lesion was debrided, cleaned, and closed with suture. Unfortunately, this area continued to exhibit signs of skin erosion.

Likewise, *monkey M* developed a large lesion in the skin and infection at a site where the wire bundle passed over the spinous process on the scapula (see oval, Fig. 4*A*) at ~5 mo after electrode implantation. To treat this lesion, an incision was made at this site and the skin debrided, cleaned, and sutured closed. Antibiotics were initiated in this monkey. Skin breakdown, however, persisted at this site. For the health of the two monkeys, the decision was made to remove the implants, ~8 and 6 mo after the original implantation of electrodes for *monkeys A* and *M*, respectively. Under sterile conditions, the encasement was removed from the titanium baseplate and the wires pulled, one by one, up and through the skin-baseplate margin. Significant forces applied to the wires were needed to extract them. In virtually all cases, the wire broke free suddenly with the anchor remaining behind. Within ~2 wk of removal of the electrode wires, the skin lesions resolved. The two monkeys were transferred to another protocol involving behavioral studies.

DISCUSSION

We implanted 29 arm muscles in each of three monkeys with bipolar intramuscular electrodes. The implants had two novel features. First, electrodes terminated with small gold anchors intended to prevent electrode migration. Accurate placement of the anchors was aided with an insertion tool through which stimulation could be delivered to verify target muscle location before deploying the anchor. Second, for two of the monkeys, we used titanium baseplates to which the electrode-connector encasement was attached. This obviated the need for using oftentimes problematic acrylic cement to secure the encasement to the skull. We adapted this method from one described by Blonde et al. (25) for mounting chambers on the skull used for brain recordings. This method was successful in maintaining healthy skin at the margins of the implant, with no signs of infection the two monkeys in which we used this system.

As far as we are aware, this is the first study to quantitatively document the stability of implanted intramuscular electrodes with electromyographic and stimulation methods. We characterized the consistency of EMG signals recorded over multiple sessions associated with the same reaching task. The patterns and amplitudes of these signals remained highly similar, as reflected by low coefficient of variation across sessions. We also documented the consistency in isometric force responses to electrical stimulation. Although somewhat more variable than EMG, stimulus thresholds and peak forces at 16 wk were not different from those recorded at 4 wk. Collectively, these findings suggest that the implanted electrodes were reasonably stable and provided reliable muscle recording and stimulation over a period of months.

Limitations

The most important limitation of our study was the inability to follow the stability of the implant over longer time periods. This came about because skin breakdown and consequent infection at particular locations led to early termination of the study. Some of these lesions

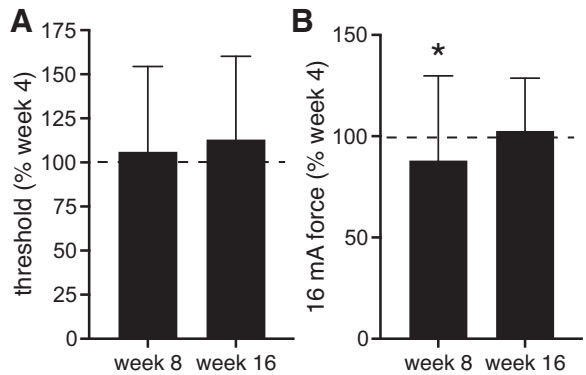

Figure 9. *A*: mean (SD) minimum (threshold) current needed to evoke a twitch response at 8 and 16 wk after electrode implantation, expressed as % of threshold measured at 4 wk. *B*: peak twitch force evoked with 16-mA stimulus pulse at 8 and 16 wk after electrode implantation, expressed as % of peak force measured at 4 wk. *Significantly different from 100% (P = 0.003). n = 111 electrodes; 55 from *monkey A*, 56 from *monkey M*.

appeared to correspond to sites with minimal subcutaneous tissue and where large electrode bundles passed over bony prominences (viz. the occipital ridge and spinous process of the scapula). This likely led to relatively high pressure between the electrode wires and neighboring tissues in these regions. Such mechanical pressure and associated irritation can provoke inflammation and tissue breakdown (31). In addition, these regions were associated with sites where all electrodes were bundled together, leading to a high density of implant material at these locations. Greater density of implant material has been shown to lead to higher levels of persistent tissue inflammation (32, 33). For future implants, therefore, it will be important to have a more dispersed arrangement of electrode leads, and to route the leads to avoid bony prominences, as much as possible. It may also be possible to reduce the diameter of the electrode leads from what we used here (outside diameter 0.33 mm) to thinner wire (e.g., 0.28 mm).

In addition, we observed tissue deterioration in the vicinity of the ground disk electrode. Although the lead to this electrode was made of biocompatible polytetrafluoroethylene, the disk itself was coated with a layer of silver-silver chloride. Silver-silver chloride can lead to toxic reactions with tissue (34, 35), which likely contributed to persistent inflammation and skin breakdown. In the future, reference electrodes will be composed of a different, more biocompatible material (e.g., titanium, Ref. 36) or silver-silver chloride coated with biocompatible membranes (37, 38).

Because we were constrained to use noninvasive methods to fix the arm for isometric force testing, there was likely some degree of variability as to how animals were positioned in the testing apparatus across sessions. Even modest variations in limb configuration leading to changes in muscle length and alteration in electrode-nerve distances could lead to marked disparities in evoked force (29, 39). Despite this, there was little systematic variation across time in evoked forces, suggesting that the implanted electrodes were reasonably stable.

Another potential limitation of our approach is that we did not use helically coiled lead wire for our electrodes. Indeed, a frequent mode of electrode failure is due to mechanical fatigue and breakage of leads because of repeated bending of wire as limbs move. Leads with helical configurations can tolerate high dynamic stresses and reduce the likelihood of mechanical fatigue (40). These leads are widely used in clinical implants for functional electrical stimulation. One drawback to using helical coiled wire, however, is that the overall diameter of the lead increases substantially. In our case (with 60 electrodes), the added thickness would have made surgical implantation substantially more challenging and would have increased the density of implanted material, perhaps encouraging tissue breakdown. We instead included substantial additional slack wire (see Fig. 4*A*) to aid in strain relief on the implanted anchors.

Finally, another possible drawback of our approach is the relatively large size of the anchors that we used (1 × 7 mm). This size made them relatively easy to handle during surgery and provided a reasonably large textured surface area to enhance shear friction and thereby tend to minimize migration. In addition, the large gold surface area ensured low interface impedance of the electrodes. However, such a size may make it difficult to implant in small muscles, such as intrinsic hand muscles. For those applications, it would seem necessary to create thinner anchors about half the length of those used in the present investigation.

Electrode Anchoring Methods

Instability and migration of implanted electrodes has long challenged investigators and clinicians. For intramuscular electrodes, many investigators have adopted the hooked-wire method originally developed for acute recording of EMG signals (41). These electrodes, however, tend to fracture at the bend in the hook, thereby limiting their long-term stability (42). Indeed, many hook wire electrodes showed substantial migration after only 1 wk of implantation (Ref. 43, cited in Ref. 44). In >1,000 intramuscular electrodes used in human patients having hooked-wire fixation, about half failed within 6 mo of implantation, mainly because of electrode migration (45).

To mitigate such displacement of electrodes, several methods have been developed. These include epimysial electrodes in which electrodes are imbedded in a Dacron or silicone sheet that is sutured to the connective tissue encompassing muscle (16, 46). The drawback to these electrodes is the added surgical time needed to suture each sheet to muscle. Also, some deep muscles do not offer accessible surfaces onto which these electrodes can be readily sutured (47). Another approach has been to add supplemental anchoring material to the electrodes. For example, polypropylene monofilaments can be affixed to the electrode to aid in securing the electrode in muscle (47, 48). The system developed by Memberg et al. (47) included a multipronged polypropylene anchor that extended from the electrode. A three-part implantation tool was needed to insert the electrodes into muscle. Overall, this approach provided secure, long-term stability of the implanted electrodes. The drawback is that the electrodes require complex prefabrication with leads cut to length and in-line connectors to attach to leads emanating from the stimulator. Furthermore, the affixed anchors and relatively thick leads (1.3 mm) make surgical tunneling of electrodes challenging if in-line connectors are not used.

In our application, the anchors were the electrodes. No prefabrication was required. Therefore, leads could be cut exactly to the required lengths in surgery and the anchors quickly secured to leads. Furthermore, no in-line connections were needed because leads were fixed to the connector board before surgery. Because tunneling only involved thin-diameter wire (0.3 mm) with no supplementary components on the distal ends, tangling or catching during tunneling was greatly minimized. In addition, only a single, simple tool was needed for insertion. Collectively, this facilitated reasonably efficient surgeries, with total surgical time of ~7.5 h for implanting 58 electrodes. This compares to 12 h required to implant 48 electrodes as reported by Park et al. (19). Finally, we believe that the period of immobilization immediately following surgery enhanced electrode stability by providing sufficient time for encapsulation and securing the anchors in place with connective tissue (44).

Nonacrylic Mount of Connector Chamber on Skull

Dental acrylic (polymethyl methacrylate) is extensively used to fix recording chambers onto the skulls of nonhuman primates for neurophysiological recordings. The acrylic itself does not adhere to bone. Instead, screws are inserted into the skull with screw heads lying ~5 mm above the surface of the skull. The dental acrylic is poured over the screws to which the cement becomes anchored. This method is efficient, inexpensive, and effective. However, because dental acrylic does not adhere to bone, and because of potential cytotoxic effects (49), small gaps can occur between bone and the acrylic. Such gaps provide an ideal environment for proliferation of bacteria that gain access at the skin-acrylic interface. Because the infection is secluded under the acrylic dome, it is difficult to treat. These infections can cause severe deterioration of the skull (22), as was the case with our first animal.

To avoid these complications, new methods have been developed using novel cement materials that minimize problems associated with dental acrylic (50) or that avoid the use of cements altogether (21, 22, 25, 50). The cementless implants use bone-compatible materials, such as titanium or polyether ether ketone, to secure chambers to the skull. It is important that the implants be custom fabricated, with CT- or MR-based imaging data, to fit the specific contours of each subject's skull to minimize gaps and promote osseointegration.

Here we adapted the method described by Blonde et al. (25) and designed a two-stage implant specific for mounting intramuscular electrode connectors within a protective chamber on the skull. The first stage involved installing a titanium baseplate with titanium bone screws. Several weeks was allowed for this platform to osseointegrate to become well anchored to the skull. In a second surgery, the baseplate was exposed, the chamber was then easily fixed to the baseplate, and electrodes were routed to and inserted into target muscles. This two-stage approach reduced surgical time associated with electrode implantation by at least 2 h. More importantly, the skin adjacent to the skull implant remained healthy and infection free for the duration of the study.

Conclusions

The electrode anchoring system we developed here provided stable EMG recording and electrically evoked responses over a period of months. The acrylic-free method for mounting the electrode connector chamber on the skull presented no complications and provided a stable platform for interfacing intramuscular electrodes with amplifiers and stimulators. Skin lesions, however, developed at sites where electrode bundles passed over bony prominences and in response to chronic inflammation associated with nonbiocompatible material used for the ground electrode. We believe these complications could readily be addressed in future implants, yielding a system that enables recording and stimulating of multiple muscles over a period of years. Such a large-scale system should help deepen our understanding of the complexities of limb motor control in both normal and impaired conditions.

ACKNOWLEDGMENTS

The authors are grateful to Lierin Cox, Chelsea Mahnk, Derek O'Neill, and Drs. C. J. Doane and Diego Celdran for animal care and surgical support. We are also grateful to Baldwin Goodell and Dr. Charles Gray (Gray Matter Research) for assistance with development of the titanium baseplate system. We gratefully acknowledge the dissections (Fig. 1) performed by Dr. Alie Buckmire. We are thankful to Drew Sheets for technical assistance.

GRANTS

This work was supported by NIH Grant R01NS102259.

DISCLOSURES

No conflicts of interest, financial or otherwise, are declared by the authors.

AUTHOR CONTRIBUTIONS

N.L.H., B.A.H., K.M.G., and A.J.F. conceived and designed research; N.L.H., B.A.H., K.M.G., and A.J.F. performed experiments; B.A.H. and A.J.F. analyzed data; N.L.H., B.A.H., and A.J.F. interpreted results of experiments; B.A.H. and A.J.F. prepared figures; N.L.H. and A.J.F. drafted manuscript; N.L.H., B.A.H., K.M.G., and A.J.F. edited and revised manuscript; N.L.H., B.A.H., K.M.G., and A.J.F. approved final version of manuscript.

REFERENCES

1. **Wood-Jones F.** *The Principles of Anatomy as Seen in the Hand*. London: J & A Churchill, 1920.
2. **Maier MA**, **Hepp-Reymond MC.** EMG activation patterns during force production in precision grip. I. Contribution of 15 finger muscles to isometric force. *Exp Brain Res* 103: 108–122, 1995. doi:10.1007/BF00241969.
3. **Schieber MH.** Muscular production of individuated finger movements: the roles of extrinsic finger muscles. *J Neurosci* 15: 284–297, 1995. doi:10.1523/JNEUROSCI.15-01-00284.1995.
4. **Fuglevand AJ.** Mechanical properties and neural control of human hand motor units. *J Physiol* 589: 5595–5602, 2011. doi:10.1113/jphysiol.2011.215236.
5. **Polit A**, **Bizzi E.** Characteristics of motor programs underlying arm movements in monkeys. *J Neurophysiol* 42: 183–194, 1979. doi:10.1152/jn.1979.42.1.183.
6. **Hogan N.** An organizing principle for a class of voluntary movements. *J Neurosci* 4: 2745–2754, 1984. doi:10.1523/JNEUROSCI.04-11-02745.1984.
7. **Hasan Z**, **Karst GM.** Muscle activity for initiation of planar, two-joint arm movements in different directions. *Exp Brain Res* 76: 651–655, 1989. doi:10.1007/BF00248921.
8. **Gottlieb GL.** The generation of the efferent command and the importance of joint compliance in fast elbow movements. *Exp Brain Res* 97: 545–550, 1994. doi:10.1007/BF00241548.
9. **Thoroughman KA**, **Shadmehr R.** Electromyographic correlates of learning an internal model of reaching movements. *J Neurosci* 19: 8573–8588, 1999. doi:10.1523/JNEUROSCI.19-19-08573.1999.
10. **Feldman AG**, **Levin MF.** The equilibrium-point hypothesis—past, present and future. *Adv Exp Med Biol* 629: 699–726, 2009. doi:10.1007/978-0-387-77064-2_38.
11. **Franklin DW**, **Wolpert DM.** Computational mechanisms of sensorimotor control. *Neuron* 72: 425–442, 2011. doi:10.1016/j.neuron.2011.10.006.
12. **DeLong MR**, **Strick PL.** Relation of basal ganglia, cerebellum, and motor cortex units to ramp and ballistic limb movements. *Brain Res* 71: 327–335, 1974. doi:10.1016/0006-8993(74)90975-5.
13. **Fetz EE**, **Cheney PD.** Postspike facilitation of forelimb muscle activity by primate corticomotoneuronal cells. *J Neurophysiol* 44: 751–772, 1980. doi:10.1152/jn.1980.44.4.751.

14. **Cheney PD**, **Fetz EE.** Comparable patterns of muscle facilitation evoked by individual corticomotoneuronal (CM) cells and by single intracortical microstimuli in primates: evidence for functional groups of CM cells. *J Neurophysiol* 53: 786–804, 1985. doi:10.1152/jn.1985.53.3.786.
15. **Lemon RN**, **Mantel GW**, **Muir RB.** Corticospinal facilitation of hand muscles during voluntary movement in the conscious monkey. *J Physiol* 381: 497–527, 1986. doi:10.1113/jphysiol.1986.sp016341.
16. **Miller LE**, **van Kan PL**, **Sinkjaer T**, **Andersen T**, **Harris GD**, **Houk JC.** Correlation of primate red nucleus discharge with muscle activity during free-form arm movements. *J Physiol* 469: 213–243, 1993. doi:10.1113/jphysiol.1993.sp019812.
17. **Shen L**, **Alexander GE.** Neural correlates of a spatial sensory-to-motor transformation in primary motor cortex. *J Neurophysiol* 77: 1171–1194, 1997. doi:10.1152/jn.1997.77.3.1171.
18. **McKiernan BJ**, **Marcario JK**, **Karrer JH**, **Cheney PD.** Correlations between corticomotoneuronal (CM) cell postspike effects and cell-target muscle covariation. *J Neurophysiol* 83: 99–115, 2000. doi:10.1152/jn.2000.83.1.99.
19. **Park MC**, **Belhaj-Saı«f A**, **Cheney PD.** Chronic recording of EMG activity from large numbers of forelimb muscles in awake macaque monkeys. *J Neurosci Methods* 96: 153–160, 2000. doi:10.1016/S0165-0270(00)00155-2.
20. **Hudson HM**, **Griffin DM**, **Belhaj-Saïf A**, **Lee SP**, **Cheney PD.** Methods for chronic recording of EMG activity from large numbers of hindlimb muscles in awake rhesus macaques. *J Neurosci Methods* 189: 153–161, 2010. doi:10.1016/j.jneumeth.2010.03.011.
21. **Adams DL**, **Economides JR**, **Jocson CM**, **Horton JC.** A biocompatible titanium headpost for stabilizing behaving monkeys. *J Neurophysiol* 98: 993–1001, 2007. doi:10.1152/jn.00102.2007.
22. **Adams DL**, **Economides JR**, **Jocson CM**, **Parker JM**, **Horton JC.** A watertight acrylic-free titanium recording chamber for electrophysiology in behaving monkeys. *J Neurophysiol* 106: 1581–1590, 2011. doi:10.1152/jn.00405.2011.
23. **Hasse BA**, **Sheets DE**, **Holly NL**, **Gothard KM**, **Fuglevand AJ.** Restoration of complex movement in the paralyzed upper limb. *J Neural Eng* 19: 046002, 2022. doi:10.1088/1741-2552/ac7ad7.
24. **Bhadra N**, **Mortimer JT.** Extraction force and tissue change during removal of a tined intramuscular electrode from rat gastrocnemius. *Ann Biomed Eng* 34: 1042–1050, 2006. doi:10.1007/s10439-006-9125-5.
25. **Blonde JD**, **Roussy M**, **Luna R**, **Mahmoudian B**, **Gulli RA**, **Barker KC**, **Lau JC**, **Martinez-Trujillo JC.** Customizable cap implants for neurophysiological experimentation. *J Neurosci Methods* 304: 103–117, 2018. doi:10.1016/j.jneumeth.2018.04.016.
26. **Buckmire AJ**, **Lockwood DR**, **Doane CJ**, **Fuglevand AJ.** Distributed stimulation increases force elicited with functional electrical stimulation. *J Neural Eng* 15: 026001, 2018. doi:10.1088/1741-2552/aa9820.
27. **Winter DA**, **Fuglevand AJ**, **Archer SE.** Crosstalk in surface electromyography: theoretical and practical estimates. *J Electromyogr Kinesiol* 4: 15–26, 1994. doi:10.1016/1050-6411(94)90023-X.
28. **Winter DA**, **Yack HJ.** EMG profiles during normal human walking: stride-to-stride and inter-subject variability. *Electroencephalogr Clin Neurophysiol* 67: 402–411, 1987. doi:10.1016/0013-4694(87)90003-4.
29. **Grill WM**, **Mortimer JT.** Stability of the input-output properties of chronically implanted multiple contact nerve cuff stimulating electrodes. *IEEE Trans Rehabil Eng* 6: 364–373, 1998. doi:10.1109/86.736150.
30. **Macias DA**, **Buckmire AJ**, **Fuglevand AJ.** Dependence of electrically-evoked force on intramuscular electrode location (Abstract). *Soc Neurosci Abstr* 2017: 781.07, 2017.
31. **Ratner BD.** The biocompatibility of implant materials. In: *Host Response to Biomaterials*, edited by Badylak S. Amsterdam: Academic Press, 2015, p. 37–51.
32. **Klinge U**, **Klosterhalfen B**, **Conze J**, **Limberg W**, **Obolenski B**, **Öttinger AP**, **Schumpelick V.** Modified mesh for hernia repair that is adapted to the physiology of the abdominal wall. *Eur J Surg* 164: 951–960, 1998. doi:10.1080/110241598750005138.
33. **Klinge U**, **Klosterhalfen B**, **Birkenhauer V**, **Junge K**, **Conze J**, **Schumpelick V.** Impact of polymer pore size on the interface scar formation in a rat model. *J Surg Res* 103: 208–214, 2002. doi:10.1006/jsre.2002.6358.
34. **Jackson WF**, **Duling BR.** Toxic effects of silver-silver chloride electrodes on vascular smooth muscle. *Circ Res* 53: 105–108, 1983. doi:10.1161/01.res.53.1.105.
35. **Yuen TG**, **Agnew WF**, **Bullara LA.** Tissue response to potential neuroprosthetic materials implanted subdurally. *Biomaterials* 8: 138–141, 1987. doi:10.1016/0142-9612(87)90103-7.
36. **Peckham PH**, **Knutson JS.** Functional electrical stimulation for neuromuscular applications. *Annu Rev Biomed Eng* 7: 327–360, 2005. doi:10.1146/annurev.bioeng.6.040803.140103.
37. **Moussy F**, **Harrison DJ.** Prevention of the rapid degradation of subcutaneously implanted Ag/AgCl reference electrodes using polymer coatings. *Anal Chem* 66: 674–679, 1994. doi:10.1021/ac00077a015.
38. **Wang B**, **Yang P**, **Ding Y**, **Qi H**, **Gao Q**, **Zhang C.** Improvement of the biocompatibility and potential stability of chronically implanted electrodes incorporating coating cell membranes. *ACS Appl Mater Interfaces* 11: 8807–8817, 2019. doi:10.1021/acsami.8b20542.
39. **Crago PE**, **Peckham PH**, **Thrope GB.** Modulation of muscle force by recruitment during intramuscular stimulation. *IEEE Trans Biomed Eng* 27: 679–684, 1980. doi:10.1109/TBME.1980.326592.
40. **Caldwell CW**, **Reswick JB.** A percutaneous wire electrode for chronic research use. *IEEE Trans Biomed Eng* 22: 429–432, 1975. doi:10.1109/tbme.1975.324516.
41. **Basmajian JV**, **Stecko G.** A new bipolar electrode for electromyography. *J Appl Physiol* 17: 849–849, 1962. doi:10.1152/jappl.1962.17.5.849.
42. **Jonsson B**, **Bagge UE.** Displacement, deformation and fracture of wire electrodes for electromyography. *Electromyography* 8: 329–347, 1968.
43. **Mortimer JT**, **Peckham PH.** Intramuscular electrical stimulation. In: *Neural Organization and Its Relevance to Prosthetics*, edited by Fields WS, Leavitt LA. Miami, FL: Symposia Specialists, 1973, p. 131–146.
44. **Bhadra N**, **Mortimer JT.** Extraction forces and tissue changes during explant of CWRU-type intramuscular electrodes from rat gastrocnemius. *Ann Biomed Eng* 25: 1017–1025, 1997. doi:10.1007/BF02648127.
45. **Marsolais EB**, **Kobetic R.** Implantation techniques and experience with percutaneous intramuscular electrodes in the lower extremities. *J Rehabil Res Dev* 23: 1–8, 1986.
46. **Grandjean PA**, **Mortimer JT.** Recruitment properties of monopolar and bipolar epimysial electrodes. *Ann Biomed Eng* 14: 53–66, 1986. doi:10.1007/BF02364648.
47. **Memberg WD**, **Peckham PH**, **Keith MW.** Surgically-implanted intramuscular electrode for an implantable neuromuscular stimulation system. *IEEE Trans Rehab Eng* 2: 80–91, 1994. doi:10.1109/86.313149.
48. **Prochazka A**, **Davis LA.** Clinical experience with reinforced, anchored intramuscular electrodes for functional neuromuscular stimulation. *J Neurosci Methods* 42: 175–184, 1992. doi:10.1016/0165-0270(92)90097-W.
49. **Dahl OE**, **Garvik LJ**, **Lyberg T.** Toxic effects of methylmethacrylate monomer on leukocytes and endothelial cells in vitro. *Acta Orthop Scand* 65: 147–153, 1994 [Erratum in *Acta Orthop Scand* 66: 387, 1995]. doi:10.3109/17453679408995423.
50. **Johnston JM**, **Cohen YE**, **Shirley H**, **Tsunada J**, **Bennur S**, **Christison-Lagay K**, **Veeder CL.** Recent refinements to cranial implants for rhesus macaques (*Macaca mulatta*). *Lab Anim (NY)* 45: 180–186, 2016. doi:10.1038/laban.997.